Nanoscale

Accepted Manuscript

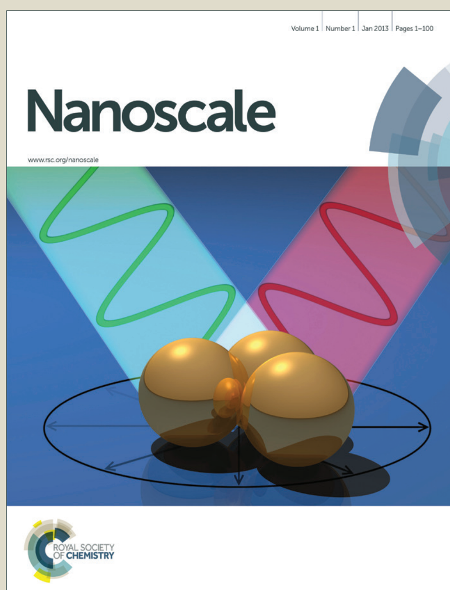

This is an *Accepted Manuscript*, which has been through the Royal Society of Chemistry peer review process and has been accepted for publication.

Accepted Manuscripts are published online shortly after acceptance, before technical editing, formatting and proof reading. Using this free service, authors can make their results available to the community, in citable form, before we publish the edited article. We will replace this *Accepted Manuscript* with the edited and formatted *Advance Article* as soon as it is available.

You can find more information about *Accepted Manuscripts* in the Information for Authors.

Please note that technical editing may introduce minor changes to the text and/or graphics, which may alter content. The journal's standard Terms & Conditions and the Ethical guidelines still apply. In no event shall the Royal Society of Chemistry be held responsible for any errors or omissions in this *Accepted Manuscript* or any consequences arising from the use of any information it contains.

ROYAL SOCIETY OF CHEMISTRY

www.rsc.org/nanoscale

Please do not adjust margins

Nanoscale

ARTICLE

Morphology and composition controlled growth of polar *c*- and nonpolar *m*-axis well-aligned ternary III-nitride nanotube arrays

Received 00th January 20xx,
Accepted 00th January 20xx

DOI: 10.1039/x0xx00000x

www.rsc.org/

Huijie Li,[*a] Guijuan Zhao,[a] Susu Kong,[a] Dongyue Han,[a] Hongyuan Wei,[a] Lianshan Wang,[a] Zhen Chen[b] and Shaoyan Yang[*a]

Control over the nanostructure morphology and growth orientation is highly demanded for the fundamental research and technological applications. Herein we report a general strategy to fabricate polar *c*- and nonpolar *m*-axis well-aligned III-nitride ternary nanotube arrays with controllable morphologies and compositions. By depositing AlN on the InN nanorod array templates and thermally removing the InN templates, InAlN nanotubes can be obtained. Polar *c*-axis and nonpolar *m*-axis nanotubes were formed on the *c*- and *r*-plane sapphire substrates, respectively. The nanotubes are single crystalline and highly ordered on the substrates, as revealed by the X-ray diffraction, electron microscopy, and selected area electron microscopy characterizations. It was found that the In droplets on top of the InN nanorods play a critical role in controlling the morphology of the nanotubes. By keeping or removing the In droplets, the obtained nanotubes exhibited both ends open or only one end open. And by varying the AlN deposition temperature, the In composition in the nanotubes can be changed from 0 to 0.29. The nanotube synthesis method is simple and can be applied to the formation of other III-nitride ternary (InGaN, and AlGaN) or quaternary (InAlGaN) alloy nanotube arrays.

1. Introduction

The III-nitride (AlN, GaN, and InN) nanostructures have been recognized as critical foundations for various nanoscale (opto)electronic devices due to their remarkable properties, such as high carrier radiative recombination rates, thermal conductivity, breakdown voltage and electron saturation velocity.[1-4] More importantly, by forming ternary alloys (AlGaN, InGaN, and InAlN), it is able to tune the energy bandgap from the deep-ultraviolet to the near-infrared region,[5,6] making them attractive for applications in solid state lightning, photovoltaics, and photoelectrochemical water splitting.[7-10] During the past decade, various nanostructures, including nanowires,[11,12] nanotips,[13] nanotubes,[14-16] and nanoflowers[17] have been synthesized for the binary III-nitrides. And very recently, ternary InGaN nanowalls,[18,19] nanowires[20], and AlGaN nanocones[21] across almost the entire composition were successfully formed and very broad tunable emissions were demonstrated. Nevertheless, the research on ternary nanostructures in other forms is still very limited. Among the one dimensional (1D) nanostructures, nanotubes are of particular importance for realizing many devices. Owing to the hollow structure, the physical properties of a nanotube are believed to combine characteristics of both two-dimensional (2D) and 1D materials.[22] And because of the extremely large surface-to-volume ratio, nanotubes are very appropriate for creating field emission,[23,24] gas storage,[25,26] and nanofluidic biochemical sensing[22] devices, etc. Although there was a previous report on the AlGaN nanotube formation,[27] the products were non-uniform and disorderly distributed on the substrates, which would complicate the device fabrication and thus is inconvenient for large-scale manufacturing.[28]

Moreover, most researches about the III-nitride nanostructures to date have focused on the polar *c*-axis of wurtzite structure, while those along the nonpolar directions (*m*- or *a*-axises) have been much less concerned. Owing to the anisotropic crystal structure, nonpolar III-nitride nanostructures are expected to be quite different from the polar ones in many physical properties, such as bandgap,[29] polarization field,[30] and elastic constants.[31] Nonpolar nanostructures are also believed to be more suitable for preparing nanogenerators,[32] photodectors,[33,34] laser diodes,[35] and high electron mobility transistors,[4] etc. For example, the output voltage of an *m*-axis InN nanowire nanogenerator can reach as high as 1V, which is almost 20 times larger than that made from a *c*-axis nanowire.[32] Therefore, control over the nanostructure growth direction is highly demanded for fundamental physics studies, as well as the potential device applications. However, up to now, only binary nonpolar III-nitride nanostructure arrays have been reported, fabrication of well-aligned ternary III-nitride nanostructure arrays with controllable growth directions has still remained as one of the foremost challenges.

[a] Key Laboratory of Semiconductor Materials Science and Beijing Key Laboratory of Low Dimensional Semiconductor Materials and Devices, Institute of Semiconductors, Chinese Academy of Sciences, P. O. Box 912, Beijing 100083, People's Republic of China. Email: hjli2009@semi.ac.cn, sh-yyang@semi.ac.cn.
[b] LatticePower (Jiangxi) Corporation, No. 699 North Aixihu Road, National High-Tech Industrial Development Zone, Nanchang, Jiangxi 330029, People's Republic of China.
†Electronic Supplementary Information (ESI) available. See DOI: 10.1039/x0xx00000x

Nanoscale Accepted Manuscript

Please do not adjust margins

Many approaches have been developed for synthesizing III-nitride nanotubes,[14-16] but only the 'epitaxial casting' method[16,36] utilizing a sacrificial nanowire/nanorod template can produce uniform and well-aligned nanotube arrays. ZnO nanowire array is the most developed template because it can be easily etched away by acid solutions or thermal reduction.[22] The main deficiency while using ZnO nanowire templates is that most of the obtained nanotubes have only one end open. But for nanofluidic applications, both-end-opened nanotubes are crucial to make both of the tube ends accessible to the fluid reservoir.[22] In our previous work, we found that InN nanorods can be utilized as ideal templates for preparing both-end-opened GaN nanotubes.[37] The other merit of InN nanorod templates is that they can be grown in the same furnace with the III-nitride epilayers without exposing the templates to the air, which is inevitable while using ZnO nanowires as the template.

In this work, we focus on the growth of InAlN nanotubes using InN nanorod templates. Among the III-nitride ternary alloys, InAlN has the broadest tunable bandgap range (from about 0.68 of InN to about 6.21 of AlN),[38-41] which has been suggested as an ideal candidate for broad-bandgap-range semiconductor optoelectronics.[42] In addition, InAlN can be lattice matched to GaN, InGaN, or ZnO at certain In contents with large band misalignment and refractive index contrast.[43,44] Therefore InAlN can be used as strain-free barriers for (opto)electronic devices based on those materials or developed as distributed Bragg reflector mirrors.[45,46] InAlN nanostructures have also been demonstrated and explored for poisonous gas sensing applications.[47] However, to our knowledge, successful synthesis of ternary InAlN nanotubes has not yet been reported. In the following sections, we will demonstrate that by using InN nanorod as templates, ordered arrays of polar *c*- and nonpolar *m*-axis ternary InAlN nanotubes with controllable morphologies and compositions can be obtained. A schematic illustration of the growth process is shown in Fig. 1. By epitaxial overgrowth of AlN layers on the InN nanorods and thermally etching the templates at high temperature, InAlN nanotube arrays can be fabricated. The incorporation of In into the nanotubes was caused by the In vapor species from the metal In droplet vaporization or InN decomposition during the AlN layer overgrowth. By varying the AlN deposition temperature, the In composition in the nanotubes can be changed from 0 to about 0.29. The nanotube synthesis method is relatively straightforward, and we believe that it can be applied to the formation of other III-nitride ternary (InGaN, and AlGaN) or quaternary (InAlGaN) alloy nanotube arrays.

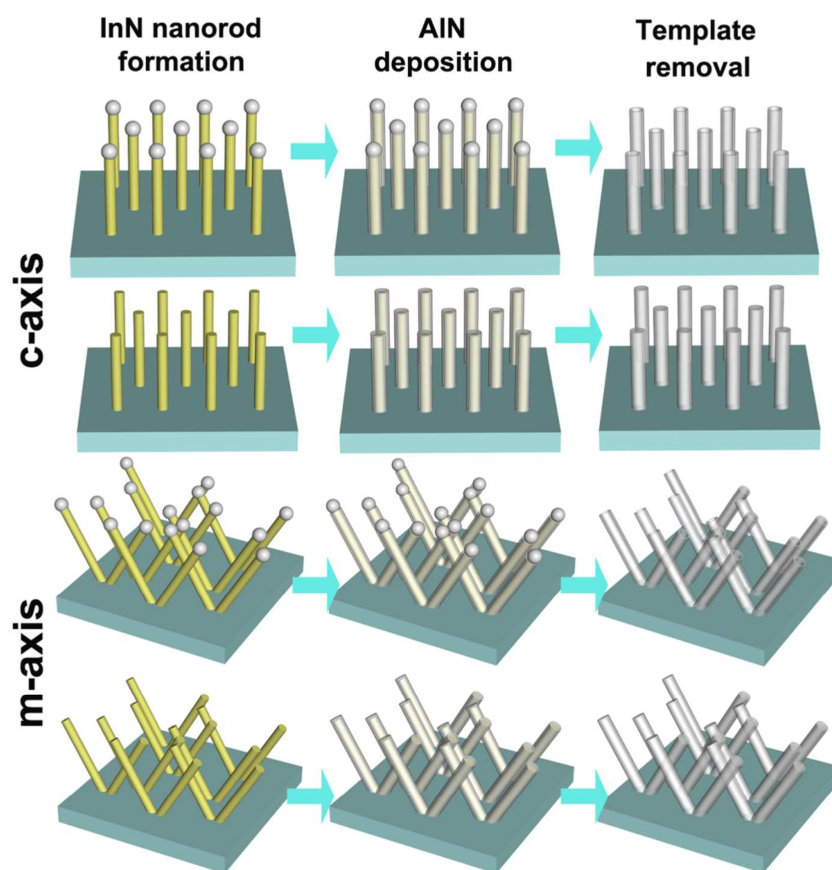

Fig. 1 Schematic illustration of the polar *c*- and nonpolar *m*-axis ternary InAlN alloy nanotube formation process.

Nanoscale Accepted Manuscript

Please do not adjust margins

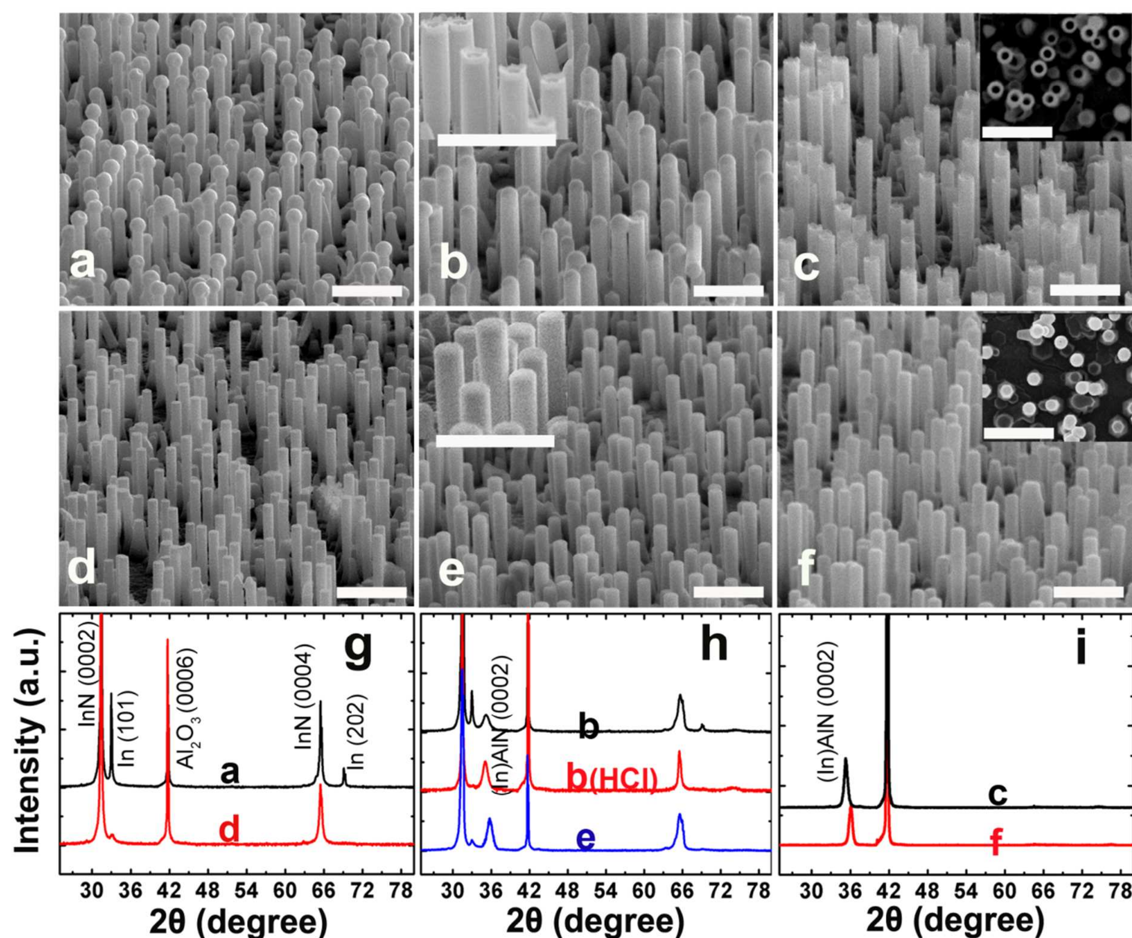

Fig. 2 SEM and XRD characterizations of the InN nanorods and InAlN nanotubes grown on *c*-plane sapphire substrates. (a), (d) The as-grown and HCl-etched InN nanorods. (b), (e) The core-sheath nanostructures after depositing AlN on the as-grown and HCl-etched nanorod templates, respectively. Insets in (b) and (e) show the morphologies of the HCl-etched AlN/InN nanostructure samples in (b) and (e), respectively. (c), (f) The nanotube arrays formed by thermally annealing the samples in (b) and (e), respectively. Insets in (c) and (f) are the corresponding cross sections of the nanotubes. (g)-(i) The corresponding XRD patterns of the nanostructure samples. The scale bars are 2 μm

2. Results and Discussion

2.1. Growth and characterization of polar *c*-axis InAlN nanotubes.

The sample growth was performed in a homemade metal-organic chemical vapor deposition (MOCVD) system, which has been described by previous researchers in our group.[17] The detailed synthesis process is described in the Experimental Section. Fig. 2 shows the scanning electron microscopy (SEM) images of the III-nitride nanostructures grown on *c*-plane sapphire substrates and the corresponding X-ray diffraction (XRD) patterns. From Fig. 2a, we can see the InN nanorods grown on *c*-plane sapphires are vertically aligned with uniform diameters and lengths of 200-400 nm and 2-3 µm, respectively. Spheres with slightly larger diameters were found on top of the nanorods, which have been demonstrated to be In droplets in previous works.[48,49] After being dipped in HCl solution for about 20 min, the droplets disappeared and flat upper surfaces of the nanorods were exposed (Fig. 2d). The X-ray diffraction (XRD) patterns of the as-grown and HCl-etched InN nanorods are shown in Fig. 2g. Metal In peaks correspond to tetragonal In (101) and (202) planes were found in the as-grown InN nanorods, and almost vanished in the HCl-etched samples. Except for the wurtzite InN (0002) and (0004) planes, no other diffraction peak of InN was observed, indicating the nanorods are grown perfectly along the [0001] direction.

AlN layers were subsequently deposited onto the InN nanorods by introducing trimethylaluminum (TMAl) and NH_3 into the chamber at 600 °C for 2 min. The chamber pressure was kept as 6.7 kPa. After the AlN deposition, the general morphology of the initial nanorods was maintained, except for the slightly increased diameters of the resulting nanostructures (Fig. 2b,e). Interestingly, it seems that AlN prefers to grow on the InN sidewalls rather than deposit on the In droplets, as indicated by the unchanged In droplet size after AlN growth.

Nanoscale Accepted Manuscript

Please do not adjust margins

Therefore the In droplets are conducive to the formation of both-end-opened nanotubes. By etching the sample in Fig. 2b with HCl solution, the In droplets disappeared and small pits were exposed on the top ends of the nanostructures (Fig. 2b inset). In comparison, no obvious morphology difference was observed for the sample in Fig. 2e with/without HCl etching. The XRD patterns of the AlN coated InN nanostructures show additional peaks as compared with the initial InN templates (Fig. 2h), which can be ascribed to the InAlN (0002) plane diffractions. The (0002) XRD peak of InAlN formed on the HCl-etched InN nanorods was found to be much closer to the (0002) AlN peak than that grown on the as-fabricated InN nanorods, which indicates the latter have larger In content than the former. Fig. 2c,f show the representative images of the obtained nanotubes by thermally removing the InN templates of the nanostructures in Fig. 2b,e, respectively. It is clear the nanotubes are vertically formed on the substrates with uniform diameter and very good alignment. The nanotubes in Fig. 2c and f exhibit open and closed top ends, respectively (Fig. 2c,f insets). As stated above, the difference was caused by the In droplets on the as-grown InN nanorods. Only (0002) XRD peaks of III-nitrides were found on the nanotubes (Fig. 2i), further proving the perfect alignment of the products. The XRD peak position of the sample in Fig. 2f is 36.02°, which corresponds to the wurtzite AlN (0002), indicating the product is pure AlN. Differently, the diffraction peak position of sample in Fig. 2c is 35.12°, which must correspond to the InAlN (0002) planes. According to previous literatures,[50,51] the variation of the unstrained InAlN lattice parameters with In content x fulfills the Vegard's rule:

$$\xi(x) = x\xi^{InN} + (1-x)\xi^{AlN}. \xi = a, c, \quad (1)$$

where a, c are the lattice parameters. Taking the unstrained lattice constants for InN (c_0 = 5.70374 Å; a_0 = 3.53774 Å) and AlN (c_0 = 4.9810 Å; a_0 = 3.1112 Å),[50,52] the In content of the InAlN nanotubes is calculated to be about 17.3%. We should note that the nanotubes were assumed to be unstrained in the calculation. However, due to the large lattice mismatch between AlN and InN (~12%), the nanotube formed on the InN templates might not be strain-free. The In composition of the nanotubes calculated by Equation (1) would be more or less different from the actual In composition. The strain status of the samples will be discussed in the following paragraph. Since no intentional In precursor was introduced into the chamber in the AlN deposition process, the incorporation of indium into the nanotubes must be due to the In vapor from the metal In droplet vaporization at the present AlN deposition temperature. At higher AlN deposition temperature, we found that the InN nanorod decomposition can also contribute to the In incorporation into the nanotubes, which will be discussed in Section 2.3.

To further analyze the microstructures of the nanotubes, transmission electron microscopy (TEM) and corresponding selected area electron diffraction (SAED) were examined (Fig. 3). The nanotubes exhibit uniform diameters and wall thickness about 200 and 20 nm, respectively. The nanotube grown from the as-fabricated InN templates has both ends open (Fig. 3a), while that prepared from the HCl-etched InN templates exhibits only one end open (Fig. 3d). These observations are consistent with the SEM results, where open and closed top ends were

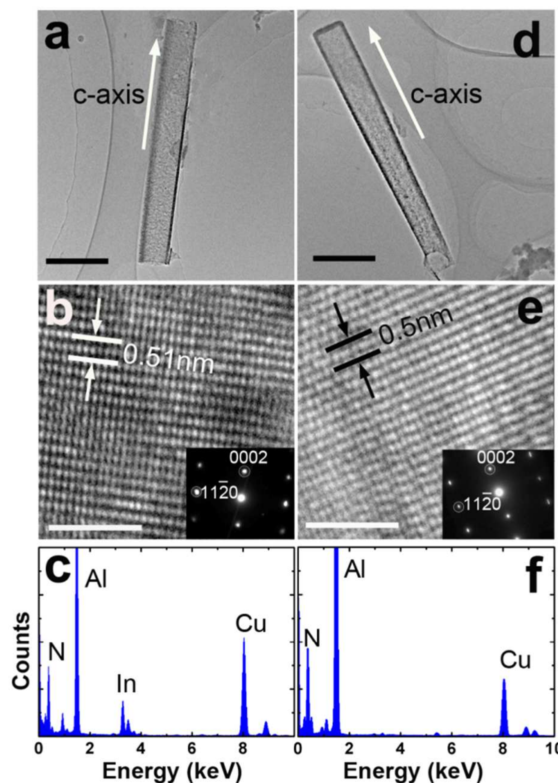

Fig. 3 Structural characterization of the nanotubes grown on c-plane sapphire substrates. (a)-(c) TEM, High-resolution TEM images, and EDXS spectrum of the nanotubes formed using the as-synthesized InN nanorod templates. (d)-(f) TEM and EDXS measurements for the nanotubes formed using the HCl-etched InN nanorod templates. Insets in b, e are the corresponding SAED patterns. Scale bars in (a), (d) are 500 nm, in (b), (e) are 2 nm.

found for the two kind nanotubes, respectively. High-resolution TEM images reveal that these nanotubes are single crystals oriented along the c-axis of wurtzite III-nitride structure (Fig. 3b,e), as also confirmed by the corresponding SAED patterns taken along the $[10\bar{1}0]$ zone axis (Fig. 3b,e insets). Along the tube axis, the lattice parameter c was found to be 0.51 and 0.5 nm for the InAlN and AlN nanotubes, respectively. And perpendicular to the tube axis, the lattice parameter a for InAlN and AlN nanotubes was found to be 0.318 and 0.31 nm, respectively. According to previous works,[50,52] the following relation for the strained InAlN alloys is fulfilled:

$$\frac{c - \left(xc_0^{InN} + (1-x)c_0^{AlN}\right)}{xc_0^{InN} + (1-x)c_0^{AlN}} = -2\frac{xC_{13}^{InN} + (1-x)C_{13}^{AlN}}{xC_{33}^{InN} + (1-x)C_{33}^{AlN}} \times \frac{a - (xa_0^{InN} + (1-x)a_0^{AlN})}{xa_0^{InN} + (1-x)a_0^{AlN}}, \quad (2)$$

where C_{13} and C_{33} are the elastic constants. Taking the elastic constant values obtained by Morales *et al.*[52] and Mánuel *et al.*[50], the In content of the InAlN nanotube was calculated to be 16.3%. This value is a little smaller than that calculated by

Nanoscale Accepted Manuscript

 This journal is © The Royal Society of Chemistry 20xx

Please do not adjust margins

Equation (1) without considering the strain status of the samples. The unstrained lattice parameter *c* obtained by Equation (1) when x = 16.3% is a little smaller than the measured value, indicating the nanotube sample was under small tensile strain (< 0.1%) along the growth direction. Since the lattice parameter of AlN is smaller than that of InN, when deposited on the InN templates, the AlN epilayer might be under tensile strain along the *c*-axis and the strain was not fully relaxed in the following growth process, resulting in the little tensile strain along the *c*-axis in the obtained products. Energy dispersive X-ray spectroscopy (EDXS) measurements were carried out to determine the In composition of the nanotubes, as shown in Fig. 3c,f. The Cu signals are generated from copper grids that support the nanotubes in the TEM measurements. The In composition of the nanotubes in Fig. 3a was found to be about 16% by calculating the relative ratio of In L_α to Al K_α peak intensities. While for the sample in Fig. 3d, no observable In signal was found, indicating the nanotube was pure AlN. These results are consistent with the XRD data, where InAlN and AlN (0002) peaks were observed for the two samples, respectively. Moreover, although it was the In droplets on top of the nanorods provided the In source for InAlN nanotube growth, the In composition along the tube axis is rather homogeneous, no progressive variation of the In content was observed (Fig. S1, ESI†). The reasons might be: (1) although most of the nanorods have similar length of about 2-3 μm, InN nanorods with very short length were also observed (Fig. S2, ESI†). The In droplets on the short nanorods may also provide the In sources in the InAlN nanotube growth process; (2) the effective diffusion length of InN at the present growth conditions is about 200 μm,[53] which is far larger than the length of the InN nanorods. Therefore in the growth process of InAlN nanotubes, no apparent In vapor pressure gradient would exist along the tube axis.

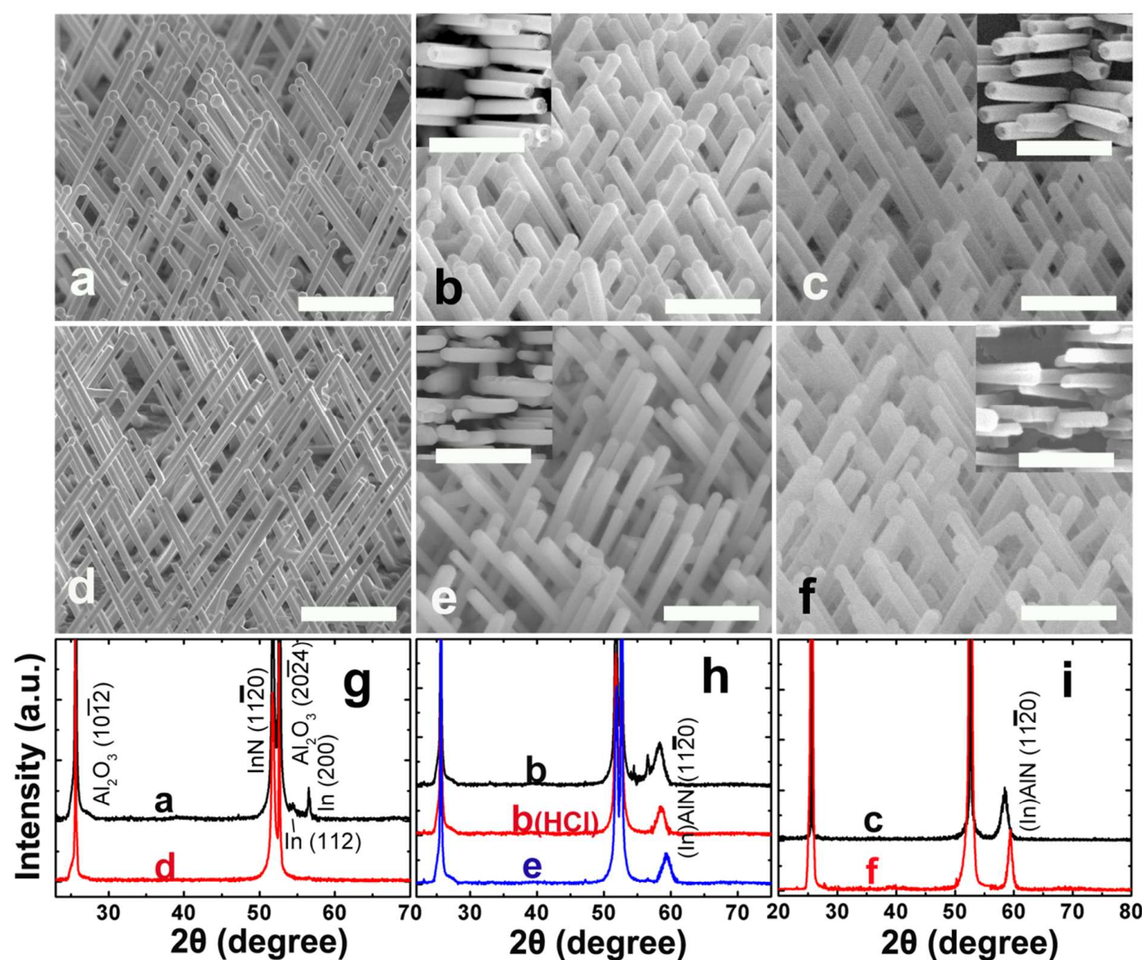

Fig. 4 SEM and XRD characterizations of the InN nanorods and InAlN nanotubes grown on *r*-plane sapphire substrates. (a), (d) The as-grown and HCl-etched InN nanorods. (b), (e) The core-sheath nanostructures after depositing AlN on the as-grown and HCl-etched nanorod templates, respectively. Insets in (b) and (e) show the morphologies of the HCl-etched AlN/InN core-sheath nanostructures. (c), (f) The nanotube arrays formed by thermally annealing the samples in (b) and (e), respectively. Insets in (c) and (f) are the corresponding SEM bird-view images of the nanotubes. (g)-(i) The corresponding XRD patterns of the nanostructure samples. The scale bars are 2 μm.

Nanoscale Accepted Manuscript

Taken together, the above measurements show that we have successfully prepared highly ordered arrays of single-crystal ternary InAlN nanotubes with both ends open and binary AlN nanotubes with only one end open. To the best of our knowledge, this is the first report of the formation of InAlN nanotubes. The nanotube synthesis process in this work is similar to the GaN nanotube formation using a ZnO nanowire template. However, the ZnO nanowires have no metal droplets on the top, the GaN epilayer could not only deposit on the sidewalls, but also on the top ends of the nanowires. Therefore most of the formed nanotubes only have one end open, both-end-opened nanotubes can rarely been obtained.[16] While for InN nanorods, the metal In droplets are simultaneously formed in the nanorod growth process, which can play an important role in controlling the morphology of the following fabricated nanotubes. By keeping or etching away the In droplets, we can choose to form III-nitride nanotubes with both ends or one end open. This feature is important for the nanofluidic applications where both-end-opened nanotubes are highly desired. Other metal catalysts, mostly noble metals, have been usually applied to grow semiconductor nanowires and always remained as droplets on top of the nanowires after the growth process.[54,55] These metal droplets may also be favorable to form both-end-opened nanotubes. But these metals are not feasible to remove after the nanotube growth, which could cause catalyst element contamination on the products. In contrast, In droplets can easily be removed at high temperatures thus are more appropriate for controlling the nanotube morphology.

2.2. Nonpolar InAlN nanotube fabrication and characterization.

Fig. 4 shows the SEM images of the nonpolar III-nitride nanostructures grown on *r*-plane sapphire substrates and the corresponding XRD patterns. Form Fig. 4a, we can see two distinct sets of InN nanorods symmetrically tilted in two opposite directions. The tilted angle between a nanorod and the substrate normal is about 30° (Fig. S3, ESI†). The mirror axis of the two set nanorods was found to be the projection of sapphire *c*-axis on the substrate surface.[56] Similar to the *c*-axis InN nanorods, each nanorod grown on *r*-plane sapphire has an In droplet on the top, which can be etched away in HCl solution (Fig. 4d). Wurtzite InN $(11\bar{2}0)$, tetragonal In (112), and In (200) XRD peaks were observed on the as-grown InN nanorods (Fig. 4g). The metal In diffraction peaks almost vanished for the HCl-etched InN nanorods. The growth direction of the InN nanorods on *r*-plane has already been determined to be *m*-axis in former work.[56] Since the angle between the *m*- and *a*-axises of wurtzite III-nitrides is 30°, the XRD peak determined by θ-2θ scan of the tilted InN nanorods would correspond to the *a*-plane InN.

After depositing the AlN epilayers at 600 °C, the diameters of the initial InN nanorods became slightly larger (Fig. 4b,e). By dipping the samples in HCl solution, the droplets on top of the nanorods in Fig. 4b disappeared and small pits were exposed (Fig. 4b inset), indicating that AlN was not coated on the In droplets. For comparison, the morphology of the sample in Fig. 4e did not change after being etched by HCl solution (Fig. 4e inset). Therefore, the In droplets can also play an important role in controlling the nonpolar nanotube morphology. XRD patterns of these samples show additional diffraction peaks correspond to hexagonal (In)AlN $(11\bar{2}0)$ planes as compared with the initial InN nanorod samples. No other diffraction peak of (In)AlN was found, indicating good epitaxy/texturing for the AlN coatings. After annealing the samples at high temperature, the obtained nanotubes maintained the initial tilted alignment of the InN nanorod templates. The tilted angle between the nanotubes and the substrate normal is also about 30°, as indicated by the side view SEM images (Fig. S3, ESI†). Similar to the *c*-plane samples, the nanotubes grown on as-synthesized and HCl-etched InN nanorods show open and closed top ends (Fig. 4c,f and insets). No diffraction peak corresponds to InN and metal In exist in the nanotube samples after high temperature annealing (Fig. 4i). The diffraction peak positions of the nanotubes in Fig. 4c and f were found to be 58.3° and 59.4°, which correspond to the InAlN and AlN $(11\bar{2}0)$ planes, respectively. Assuming the nanotubes are strain-free, the In composition of the InAlN nanotubes was calculated to be 12% from Equation (1).

To further investigate the epitaxial relationship between the nanotubes and the substrate, SEM measurements were taken along the direction which was perpendicular to the sapphire *c*-axis and tilted 30° toward the substrate normal. From this detecting direction, the cross section of a nanotube can readily be seen (Fig. 5a,b), further proving that the angle between a nanotube and the substrate normal is about 30°. The nanotubes, either with an open or closed top end, have a pentagonal cross section, which is similar to the InN nanorod templates grown on *r*-plane sapphire substrates (Fig. 5c). Most of the nanotubes have an abrupt (0001) face perpendicular to the mirror axis of the two set nanotubes. The other side faces of the nanotubes exhibit nonpolar or semipolar surfaces. The pentagonal cross sections have always been found in the nonpolar III-nitride nanowires, which was believed to be caused by the anisotropic growth rates of the different side facets. The growth rates of the $(000\bar{1})$, nonpolar, and semipolar facets are much lower than that of the (0001) facet, leading to the appearance of these facets in the *m*-axis nanostructures.[57,58] For a more clear view, a schematic illustration of the nanotubes on the *r*-plane sapphire was shown in Fig. 5d. The nanotubes basically inherited the morphology and growth direction of the initial InN nanorod templates. XRD θ-2θ scan measurements were taken by setting the mirror axis of the nanotubes parallel to the X-ray incident plane while keeping the chi angle of the substrate at 30° (Fig. 5e). From this configuration, the top surfaces of the nanotubes were adjusted to be horizontal. Diffraction peaks correspond to $(10\bar{1}0)$ III-nitride planes were found for the products, indicating the nanotubes were grown along the nonpolar *m*-axis. TEM images of the nanotubes fabricated using the as-synthesized and HCl-etched *m*-axis InN nanorods are shown in Fig. 6. Both ends and only one end opened nanotubes with uniform diameter and wall thickness can readily be seen for the two samples. High-resolution TEM images show exactly the $(10\bar{1}0)$ lattice plane perpendicular to the tube axis (Fig. 6b,e). For the sample in Fig. 6d, the perpendicular interplanar distances of 0.269 nm and 0.156 nm match well with the $d_{10\bar{1}0}$ and $d_{11\bar{2}0}$ spacings of wurtzite AlN, respectively. While for the nanotubes in Fig. 6a, the corresponding lattice parameters are slightly larger, which is caused by the In incorporation into the tubes. A clear sixfold symmetry in SAED

Nanoscale Accepted Manuscript

This journal is © The Royal Society of Chemistry 20xx

Please do not adjust margins

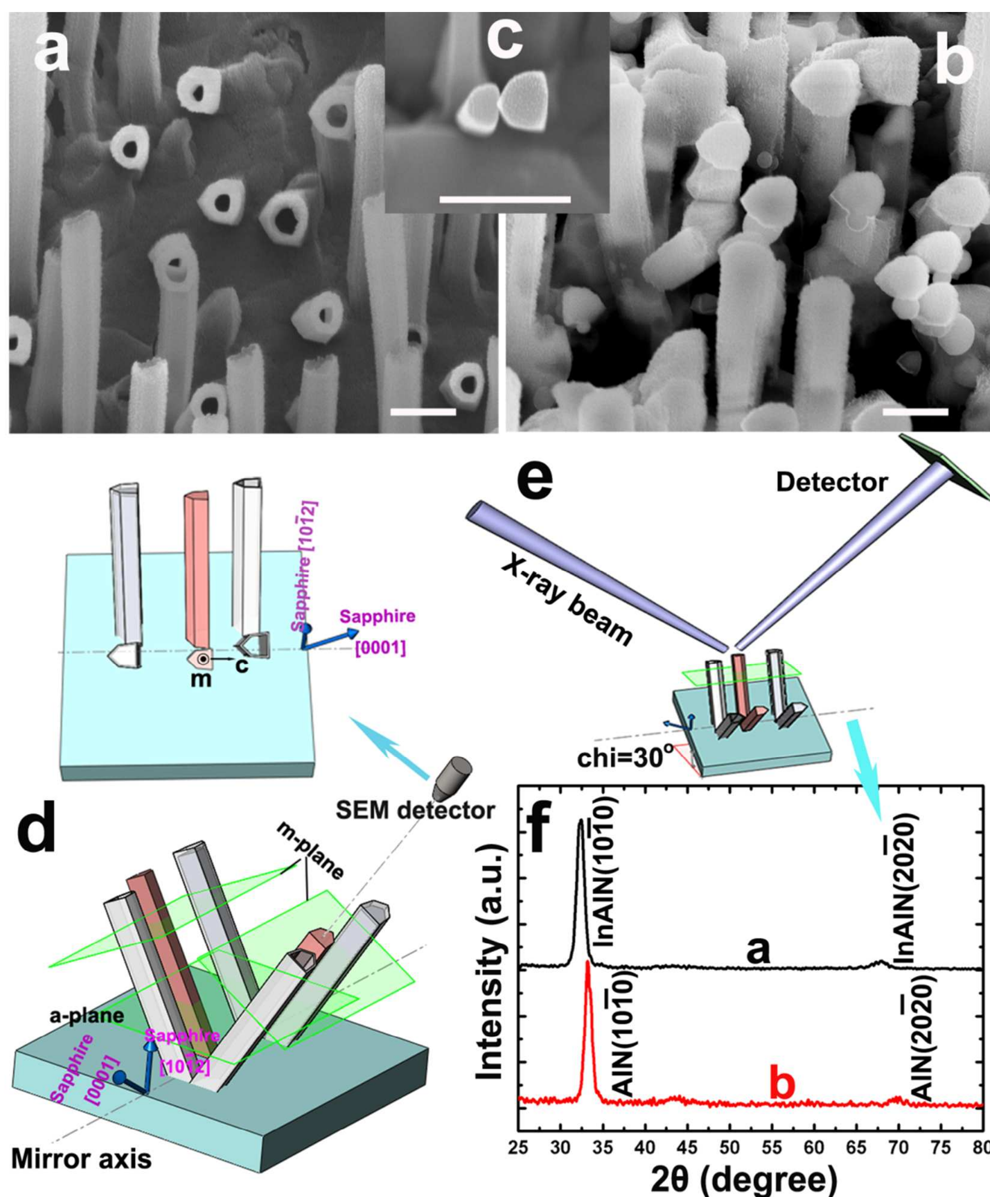

Fig. 5 (a), (b) Cross-sections of the nanotubes formed on *r*-plane sapphires using the as-synthesized and HCl-etched InN nanorod templates. (c) Cross-sections of the HCl-etched InN nanorods grown on *r*-plane sapphire substrates. (d) Schematic illustration of the epitaxial relationship between the nanostructures and the *r*-plane sapphires. (e) Schematic illustration of the XRD apparatus configuration to determine the crystal orientations of the nanotubes. (f) The corresponding XRD patterns of the nanotubes. Scale bars are 500 nm.

patterns (Fig. 6b,e insets) taken along the [0001] zone axis affirms their single crystallinity. From the alignment of the real space images and the diffraction patterns, the nanotubes were determined to be oriented along the $[10\bar{1}0]$ direction (*m*-axis), which is consistent with the XRD measurements. EDXS measurements indicate the In composition of the both-end-opened nanotubes was about 13%. While for the one-end-opened nanotubes, no observable In signal was found. These results are in agreement with the In compositions deduced from the XRD peaks and Equation (1).

2.3. Effect of the AlN deposition temperature on the nanotube morphology and composition.

The nanotube morphology grown from the HCl-etched InN nanorod templates did not change much while the AlN deposition temperature was varied from 500 to 650 °C. Similarly, no obvious morphology difference was observed when AlN was deposited at 500 ~ 600 °C using the as-synthesized InN nanorods. But at 620 °C or higher temperature, In droplets were frequently found on the

Nanoscale Accepted Manuscript

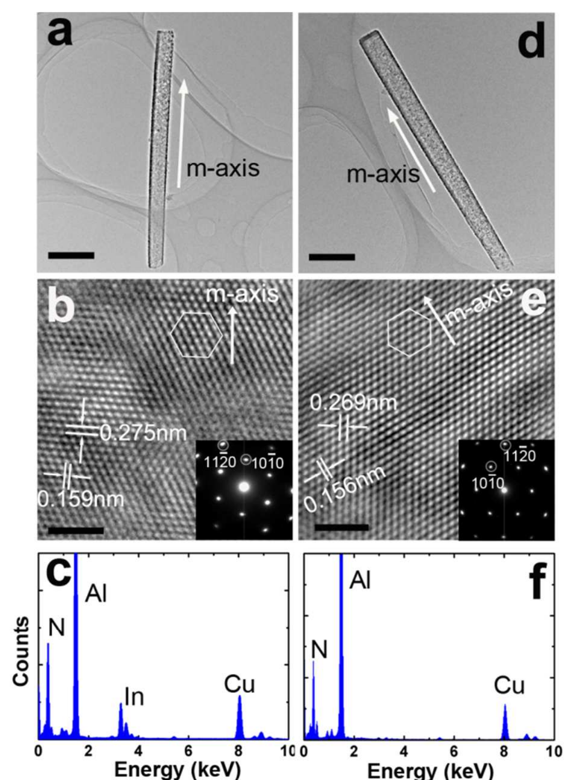

Fig. 6 Structural characterization of the nanotubes grown on *r*-plane sapphire substrates. (a)-(c) TEM, High-resolution TEM images, and EDXS spectrum of the nanotubes formed using the as-synthesized InN nanorod templates. (d)-(f) TEM and EDXS measurements for the nanotubes formed using the HCl-etched InN nanorod templates. Insets in b, e are the corresponding SAED patterns. Scale bars in (a), (d) are 500 nm, in (b), (e) are 2 nm.

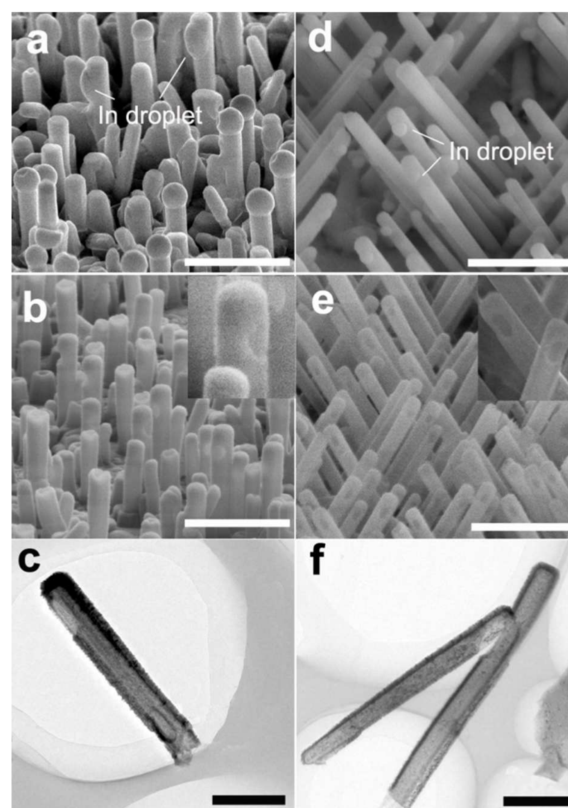

Fig. 7 The formed nanostructures when AlN was deposited at 620 °C. (a), (d) The AlN coated InN nanostructures formed on *c*- and *r*-plane sapphire substrates, respectively. (b), (e) SEM images of the obtained nanotubes by thermally annealing the samples in (a) and (d) respectively. (c), (f) TEM images of the nanotubes in (b) and (e), respectively. Insets in (b), (e) are the enlarged view of the nanotubes. Scale bars in (c), (f) are 500 nm, while that in other images are 2 μm.

sidewalls of the AlN coated InN nanostructures (Fig. 7a,d). It is because that the decomposition of InN becomes severer at higher temperatures. The upper part of a nanorod decomposed and cannot hold the In droplet anymore. The In droplets subsequently flew down to the sidewalls and were sustained by the following grown AlN epilayers. By dipping the samples in HCl solutions, small holes appeared at the previous In droplet positions (Fig. S4, ESI†). SEM and TEM images of the obtained nanotubes grown on the as-synthesized InN nanorods at 620 °C are shown in Fig. 7. It can be seen that some of the nanotubes exhibit closed top ends but have open holes on the sidewalls. At growth temperature above 670 °C, the InN nanorods were so severely deteriorated that no ordered nanotube arrays can be obtained (Fig. S5, ESI†).

XRD measurements were carried out on the nanotubes grown at different temperatures. The diffraction peaks of both the polar and nonpolar nanotubes progressively shift toward the lower angle side as the temperature increases (Fig. S6, ESI†). It is resulted from the increasing lattice parameters with increasing In/Al ratio due to the larger atomic radius of In than Al. From Equation (1), the In composition of the nanotubes was calculated and shown in Fig. 8. We can see that when the AlN deposition temperature exceeds 600 °C, apparent In contents were found in the one-end-opened nanotubes fabricated using the HCl-etched InN nanorods. It must be due to that the decomposition of the InN nanorod templates became severer at higher temperature, the vapor pressure of the generated In vapor became significantly higher and lead to the obvious In incorporation into the nanotubes. For the *c*- axis nanotubes grown from the as-synthesized InN nanorods, the In content increased progressively from nearly 0 at 480 °C to about 0.29 at 650 °C (Fig. 8a). It is well known that while the growth temperature was increased, the vaporization of the In droplets or the decomposition of the InN nanorods were accelerated, therefore the In species vapor pressure became larger. Since the Al vapor pressure was maintained as constant, the In content of the obtained nanotubes should be higher at the elevated AlN growth temperature. As is seen from Fig. 8, at the same growth temperature, the In composition of the nanotubes grown on the HCl-etched InN templates is smaller than that grown on the as-synthesized InN templates due to the absence of In droplet. For the nonpolar nanotubes, the In content is a little smaller than that of the polar nanotubes at the same growth temperature (Fig. 8b). It might be caused by the different In

Nanoscale Accepted Manuscript

 This journal is © The Royal Society of Chemistry 20xx

Please do not adjust margins

incorporation efficiency in different InAlN crystal orientations. We should note the strain status of the samples was not considered when calculating the In compositions by Equation (1). Therefore the In composition would deviate from the actual values. To get the precise In contents of the samples, both the lattice parameters *c* and *a* are needed. However, the nanotubes are not very dense (~10^8 cm^{-2}), it is difficult to obtain both the lattice constants by asymmetric or skew diffractions. SEM-EDXS was carried out on several samples to obtain the In contents (See Fig. S7 and Table S1, ESI†). Before the measurements, the nanotubes were transferred to Cu substrates in order to eliminate the effect of the sapphire substrates. Almost all the In compositions obtained by SEM-EDXS are a little smaller than those obtained by the XRD measurements, which might be caused by that the tensile strain along the growth direction induced in the nanotube growth process was not totally relaxed.

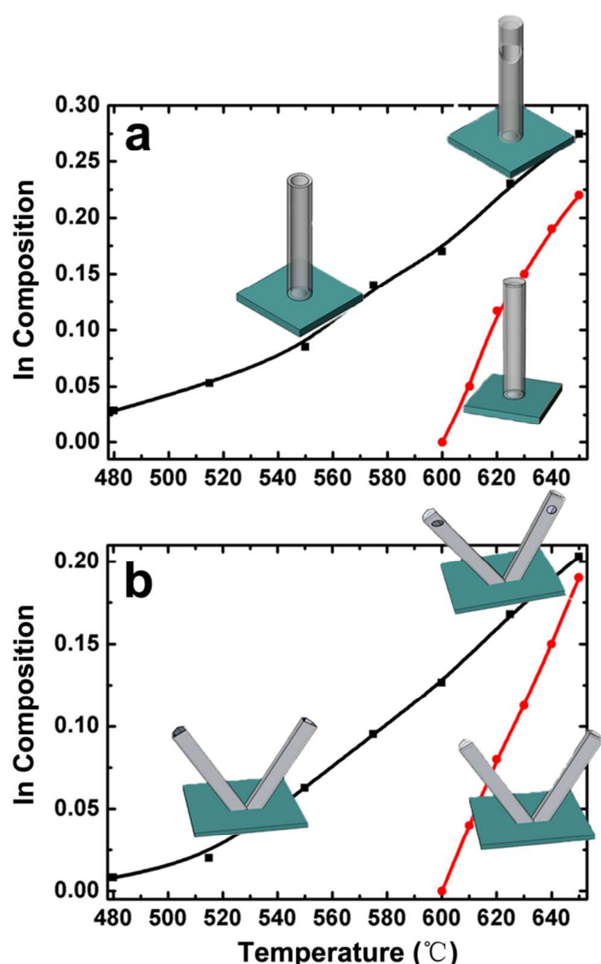

Fig. 8 The In compositions of the (a) *c*-axis and (b) *m*-axis nanotubes grown at different temperatures. The black lines represent the results of the nanotubes grown on the as-synthesized InN nanorods, while the red lines are the compositions of the nanotubes formed on the HCl-etched InN nanorods. The insets are the schematic illustrations of the nanotube morphologies formed at different conditions.

Moreover, it should be noted that at the AlN deposition temperature, the In vapor pressure from the vaporization of In droplets is about 10^{-4} Pa,[59] which is only ~1% of the Al partial pressure in the chamber. The In composition in the nanotube products is significantly higher than the In/Al vapor pressure ratio. The reason is not clear right now. In addition, InAlN nanotubes with higher In content can be obtained by introducing trimethylindium (TMIn) into the chamber in the AlN deposition process. For example, when the In/Al inlet ratio is 1:1, the In composition in the synthesized nanotubes is about 50% (Fig. S8, ESI†). However, the main purpose of this work is to control the morphology and growth orientation of the nanotubes, growth of nanotubes over the large composition range is beyond the scope of this work. More growth mechanisms and physical properties of InAlN nanotubes across almost the entire composition range will be presented in future work.

3. Conclusion

In summary, well-aligned InAlN nanotubes with both polar and nonpolar growth directions have been synthesized for the first time. The nanotubes were grown in a MOCVD furnace using the 'epitaxial casting' approach. InN nanorods grown on *c*- and *r*-plane sapphire substrates were explored as the templates for formation of polar and nonpolar InAlN nanotubes, respectively. We found that the In droplets on the InN nanorods play a critical role in controlling the morphology of the formed nanotubes. Using the nanorod templates with or without In droplets, InAlN nanotubes with both ends or only one end open can be obtained. By varying AlN deposition temperature, nanotubes with different morphologies and In compositions from 0 to 0.29 could be obtained. The MOCVD process for fabrication nanotubes is entirely compatible with the current III-nitride thin-film technology and the products are highly ordered on the substrates, which would lead to easy scale-up and device integration. The ability to control the nanotube morphology, polarity, and composition could offer opportunities for further fundamental research and various technological applications. The successful preparation of ternary InAlN nanotubes using InN nanorod templates suggests it is possible to prepare nanotubes of other ternary or even quaternary III-nitride alloys.

4. Experimental

The InN nanorods were grown in a homemade MOCVD system by a self-catalyzed method with the assistance of Zn dopants. For growth of *c*- and *m*-axis InN nanorods, *c*- and *r*-plane sapphires were respectively used as the substrates. Before growth, the sapphire wafer was cleaned under a hydrogen flow at 1050 °C for 20 min. Subsequently, the substrate was nitridized for 3 min under a mixed gas of H_2 and NH_3 with a flow rate of 3 SLM (standard litre per minute), respectively. Then the growth temperature was set to 530 °C for InN nanorod growth. The reactions were carried out at atmospheric pressure. TMIn and NH_3 were used as precursors, and diethylzinc (DEZn) was dopant. After the growth of InN nanorods, the furnace was cooled to room temperature and the samples were taken out of the chamber. Some of the InN samples were etched in diluted HCl solution for 20 min to remove the In droplets. More details about the growth process and characterizations of the nanorods can be found in previous literatures.[48,56]

Nanoscale Accepted Manuscript

Before the AlN deposition, the furnace was heated under a hydrogen flow at 1050 °C for 30 min to remove the residual InN and In droplets. Then the InN nanorod templates were placed inside the chamber and heated to 500-650 °C under a mixed gas of N_2 and NH_3 with a flow rate of 3 SLM (standard liter per minute), respectively. The AlN deposition was carried out at 6.7 kPa with TMAl and NH_3 as the precursors. The TMAl flow rate was 20 μmol/min and the deposition process lasted for 2 min. No intended In precursors were introduced in this growth step. After the AlN layer deposition, the furnace was heated up to 1000 °C with a ramp rate of 50 °C/min. Then the temperature was kept for 10 min to thermally remove the InN nanorod templates.

The morphologies of the samples were examined by scanning electron microscopy (SEM: Nova NanoSEM 650). The SEM was equipped with an energy-dispersive X-ray spectrometer (METEK). The spectra were collected at an accelerating voltage of 20 kV. The nanotubes were transferred to Cu substrates before the SEM-EDXS measurements to eliminate the influence of the sapphire substrates. The crystal structure of the products was characterized by XRD (Philips X'pert Pro X-ray diffractometer) with Cu Kα radiation of 0.15406 nm. The nanotubes were dispersed onto copper grids possessing an amorphous carbon film and further characterized with a high-resolution transmission electron microscope (HR-TEM: JEM 2100F, 200 kV) attached to an energy-dispersive X-ray spectrometer. The TEM-EDXS spectra were collected from a ~10 × 10 nm^2 area. To calculate the In and Al atom ratio, the background-subtracted In L and Al K lines were analyzed using the energy-dispersive X-ray analysis software's standardless-quantification mode, and have an absolute error of ~2%.

Acknowledgements

This work was jointly supported by National Science Foundation of China (Nos. 91233111, 61274041, 11275228, 61504128, 61504129), Special Funds for Major State Basic Research Project (973 program) of China (No.2012CB619305), 863 High Technology R&D Program of China (Nos. 2014AA032603, 2014AA032609), and Guangdong Provincial Special Fund for LED Industrial Development (2012A080302003).

Notes and references

1 W. Guo, M. Zhang, A. Banerjee and P. Bhattacharya, *Nano Lett.*, 2010, **10**, 3355-3359.
2 N. u. H. Alvi, P. E. D. S. Rodriguez, V. J. Gómez, P. Kumar, M. Willander and R. Nötzel, *Appl. Phys. Express*, 2013, **6**, 115201.
3 J. H. Park, M. H. Kim, S. Kissinger and C. R. Lee, *Nanoscale*, 2013, **5**, 2959-2966.
4 Y. Li, J. Xiang, F. Qian, S. Gradečak, Y. Wu, H. Yan, D. A. Blom and C. M. Lieber, *Nano Lett.*, 2006, **6**, 1468-1473.
5 Y. Taniyasu, M. Kasu and T. Makimoto, *Nature*, 2006, **441**, 325-328.
6 T. Matsuoka, H. Okamoto, M. Nakao, H. Harima and E. Kurimoto, *Appl. Phys. Lett.*, 2002, **81**, 1246.
7 N. u. H. Alvi, P. E. D. Soto Rodriguez, P. Aseev, V. J. Gómez, A. u. H. Alvi, W. u. Hassan, M. Willander and R. Nötzel, *Nano Energy*, 2015, **13**, 291-297.
8 L. Caccamo, J. Hartmann, C. Fabrega, S. Estrade, G. Lilienkamp, J. D. Prades, M. W. Hoffmann, J. Ledig, A. Wagner, X. Wang, L. Lopez-Conesa, F. Peiro, J. M. Rebled, H. H. Wehmann, W. Daum, H. Shen and A. Waag, *ACS Appl. Mater. Interfaces*, 2014, **6**, 2235-2240.
9 J. H. Choi, E. H. Cho, Y. S. Lee, M.-B. Shim, H. Y. Ahn, C.-W. Baik, E. H. Lee, K. Kim, T.-H. Kim, S. Kim, K.-S. Cho, J. Yoon, M. Kim and S. Hwang, *Adv. Opt. Mater.*, 2014, **2**, 267-274.
10 S. L. Howell, S. Padalkar, K. Yoon, Q. Li, D. D. Koleske, J. J. Wierer, G. T. Wang and L. J. Lauhon, *Nano Lett.*, 2013, **13**, 5123-5128.
11 S. W. Kim, Y. H. Park, I. Kim, T. E. Park, B. W. Kwon, W. K. Choi and H. J. Choi, *Nanoscale*, 2013, **5**, 8550-8554.
12 Y.-B. Tang, X.-H. Bo, J. Xu, Y.-L. Cao, Z.-H. Chen, H.-S. Song, C.-P. Liu, T.-F. Hung, W.-J. Zhang, H.-M. Cheng, I. Bello, S.-T. Lee and C.-S. Lee, *ACS Nano*, 2011, **5**, 3591-3598.
13 S. C. Shi, C. F. Chen, S. Chattopadhyay, Z. H. Lan, K. H. Chen and L. C. Chen, *Adv. Funct. Mater.*, 2005, **15**, 781-786.
14 L.-W. Yin, Y. Bando, Y.-C. Zhu, M.-S. Li, C.-C. Tang and D. Golberg, *Adv. Mater.*, 2005, **17**, 213.
15 L.-W. Yin, Y. Bando, Y.-C. Zhu, D. Golberg and M.-S. Li, *Adv. Mater.*, 2004, **16**, 929.
16 J. Goldberger, R. He, Y. Zhang, S. Lee, H. Yan, H.-J. Choi and P. D. Yang, *Nature*, 2003, **422**, 599.
17 T.-T. Kang, X. Liu, R. Q. Zhang, W. G. Hu, G. Cong, F.-A. Zhao and Q. Zhu, *Appl. Phys. Lett.*, 2006, **89**, 071113.
18 N. H. Alvi, P. E. D. Soto Rodriguez, P. Kumar, V. J. Gómez, P. Aseev, A. H. Alvi, M. A. Alvi, M. Willander and R. Nötzel, *Appl. Phys. Lett.*, 2014, **104**, 223104.
19 P. E. D. Soto Rodriguez, P. Kumar, V. J. Gómez, N. H. Alvi, J. M. Mánuel, F. M. Morales, J. J. Jiménez, R. García, E. Calleja and R. Nötzel, *Appl. Phys. Lett.*, 2013, **102**, 173105.
20 T. Kuykendall, P. Ulrich, S. Aloni and P. Yang, *Nat. Mater.*, 2007, **6**, 951-956.
21 C. He, Q. Wu, X. Wang, Y. Zhang, L. Yang, N. Liu, Y. Zhao, Y. Lu and Z. Hu, *ACS Nano*, 2011, **5**, 1291-1296.
22 J. Goldberger, R. Fan and P. D. Yang, *Acc. Chem. Res.*, 2006, **39**, 239-248.
23 V. N. Tondare, C. Balasubramanian, S. V. Shende, D. S. Joag, V. P. Godbole, S. V. Bhoraskar and M. Bhadbhade, *Appl. Phys. Lett.*, 2002, **80**, 4813.
24 S. Hou, J. Zhang, Z. Shen, X. Zhao and Z. Xue, *Physica E*, 2005, **27**, 45-50.
25 H.-M. Cheng, Q.-H. Yang and C. Liu, *Carbon*, 2001, **39**, 1447-1454.
26 Q. Wang, Q. Sun, P. Jena and Y. Kawazoe, *ACS Nano*, 2009, **3**, 621-626.
27 H. K. Seong, Y. Lee, J. Y. Kim, Y. K. Byeun, K. S. Han, J. G. Park and H. J. Choi, *Adv. Mater.*, 2006, **18**, 3019-3023.
28 R. S. Chen, S. W. Wang, Z. H. Lan, J. T. Tsai, C. T. Wu, L. C. Chen, K. H. Chen, Y. S. Huang and C. C. Chen, *Small*, 2008, **4**, 925-929.
29 T. Kuykendall, P. J. Pauzauskie, Y. Zhang, J. Goldberger, D. Sirbuly, J. Denlinger and P. D. Yang, *Nat. Mater.*, 2004, **3**, 524-528.
30 F. Scholz, *Semicond. Sci. Technol.*, 2012, **27**, 024002.
31 R. A. Bernal, R. Agrawal, B. Peng, K. A. Bertness, N. A. Sanford, A. V. Davydov and H. D. Espinosa, *Nano Lett.*, 2011, **11**, 548-555.
32 C. T. Huang, J. Song, C. M. Tsai, W. F. Lee, D. H. Lien, Z. Gao, Y. Hao, L. J. Chen and Z. L. Wang, *Adv. Mater.*, 2010, **22**, 4008-4013.

Nanoscale Accepted Manuscript

This journal is © The Royal Society of Chemistry 20xx

33 R.-S. Chen, H.-Y. Chen, C.-Y. Lu, K.-H. Chen, C.-P. Chen, L.-C. Chen and Y.-J. Yang, *Appl. Phys. Lett.*, 2007, **91**, 223106.
34 X. Wang, Y. Zhang, X. Chen, M. He, C. Liu, Y. Yin, X. Zou and S. Li, *Nanoscale*, 2014, **6**, 12009-12017.
35 S. Gradečak, F. Qian, Y. Li, H.-G. Park and C. M. Lieber, *Appl. Phys. Lett.*, 2005, **87**, 173111.
36 S. Jiang, J. Zhang, X. Qi, M. He and J. Li, *CrystEngComm*, 2013, **15**, 9837.
37 H. Li, C. Liu, G. Liu, H. wei, C. Jiao, J. Wang, H. Zhang, D. d. Jin, Y. Feng, S. Yang, L. Wang, Q. Zhu and Z.-G. Wang, *J. Crystal Growth*, 2014, **389**, 1-4.
38 L. F. Jiang, W. Z. Shen and Q. X. Guo, *J. Appl. Phys.*, 2009, **106**, 013515.
39 P. Schley, R. Goldhahn, A. T. Winzer, G. Gobsch, V. Cimalla, O. Ambacher, H. Lu, W. J. Schaff, M. Kurouchi, Y. Nanishi, M. Rakel, C. Cobet and N. Esser, *Phys. Rev. B*, 2007, **75**, 205204.
40 E. Sakalauskas, H. Behmenburg, C. Hums, P. Schley, G. Rossbach, C. Giesen, M. Heuken, H. Kalisch, R. H. Jansen, J. Bläsing, A. Dadgar, A. Krost and R. Goldhahn, *J. Phys. D: Appl. Phys.*, 2010, **43**, 365102.
41 E. Sakalauskas, B. Reuters, L. R. Khoshroo, H. Kalisch, M. Heuken, A. Vescan, M. Röppischer, C. Cobet, G. Gobsch and R. Goldhahn, *J. Appl. Phys.*, 2011, **110**, 013102.
42 C.-L. Hsiao, J. Palisaitis, M. Junaid, R.-S. Chen, P. O. Å. Persson, P. Sandström, P.-O. Holtz, L. Hultman and J. Birch, *Appl. Phys. Express*, 2011, **4**, 115002.
43 C. Durand, C. Bougerol, J.-F. Carlin, G. Rossbach, F. Godel, J. Eymery, P.-H. Jouneau, A. Mukhtarova, R. Butté and N. Grandjean, *ACS Photonics*, 2014, **1**, 38-46.
44 T. Kajima, A. Kobayashi, K. Ueno, J. Ohta, H. Fujioka and M. Oshima, *Appl. Phys. Express*, 2013, **6**, 021003.
45 G. Cosendey, A. Castiglia, G. Rossbach, J.-F. o. Carlin and N. Grandjean, *Appl. Phys. Lett.*, 2012, **101**, 151113.
46 J. F. Carlin and M. Ilegems, *Appl. Phys. Lett.*, 2003, **83**, 668.
47 W. Y. Weng, S. J. Chang, T. J. Hsueh, C. L. Hsu, M. J. Li and W. C. Lai, *Sens. Actuators B*, 2009, **140**, 139-142.
48 H. Song, A. Yang, R. Zhang, Y. Guo, H. Wei, G. Zheng, S. Yang, X. Liu, Q. Zhu and Z. Wang, *Cryst. Growth Des.*, 2009, **9**, 3292-3295.
49 H. Song, Y. Guo, A. Yang, H. Wei, X. Xu, J. Liu, S. Yang, X. Liu, Q. Zhu and Z. Wang, *CrystEngComm*, 2010, **12**, 3936-3941.
50 J. M. Mánuel, F. M. Morales, J. G. Lozano, D. González, R. García, T. Lim, L. Kirste, R. Aidam and O. Ambacher, *Acta Mater.*, 2010, **58**, 4120-4125.
51 F. M. Morales, J. M. Mánuel, R. García, B. Reuters, H. Kalisch and A. Vescan, *J. Phys. D: Appl. Phys.*, 2013, **46**, 245502.
52 F. M. Morales, D. González, J. G. Lozano, R. García, S. Hauguth-Frank, V. Lebedev, V. Cimalla and O. Ambacher, *Acta Mater.*, 2009, **57**, 5681-5692.
53 T. Shioda, M. Sugiyama, Y. Shimogaki and Y. Nakano, *Appl. Phys. Express*, 2008, **1**, 071102.
54 Y.-B. Tang, X.-H. Bo, C.-S. Lee, H.-T. Cong, H.-M. Cheng, Z.-H. Chen, W.-J. Zhang, I. Bello and S.-T. Lee, *Adv. Funct. Mater.*, 2008, **18**, 3515-3522.
55 G. Koley, Z. Cai, E. B. Quddus, J. Liu, M. Qazi and R. A. Webb, *Nanotechnology*, 2011, **22**, 295701.
56 B. Zhang, H. Song, X. Xu, J. Liu, J. Wang, X. Liu, S. Yang, Q. Zhu and Z. Wang, *Nanotechnology*, 2011, **22**, 235603.
57 C. Chen, T. Yan, W. Hsiang and M. M. C. Chou, *Mater. Lett.*, 2014, **130**, 271-273.
58 Y. Lin, B. Leung, Q. Li, J. J. Figiel and G. T. Wang, *J. Cryst. Growth*, 2015, **427**, 67-71.
59 F. Geiger, C. A. Busse and R. I. Loehrke, *Int. J. Thermophys.*, 1986, **8**, 425-436.

Nanoscale Accepted Manuscript